Обзор ArXiv: astro-ph, 10-14 августа 2020

От Сильченко О.К.

ArXiv: 2008.05486

The Kinematics and Dark Matter Fractions of TNG50 Galaxies at $z = 2$ from an Observational Perspective

Hannah Übler[1], Shy Genel[2,3], Amiel Sternberg[4,2,1], Reinhard Genzel[1,5], Sedona H. Price[1], Natascha M. Förster Schreiber[1], Taro T. Shimizu[1], Annalisa Pillepich[6], Dylan Nelson[7], Andreas Burkert[1,8], Ric Davies[1], Lars Hernquist[9], Philipp Lang[6], Dieter Lutz[1], Rüdiger Pakmor[7], and Linda J. Tacconi[1]

[1] *Max-Planck-Institut für extraterrestrische Physik, Gießenbachstraße 1, 85748 Garching bei München, Germany*
[2] *Center for Computational Astrophysics, Flatiron Institute, 162 Fifth Avenue, New York, NY 10010, USA*
[3] *Columbia Astrophysics Laboratory, Columbia University, 550 West 120th Street, New York, NY 10027, USA*
[4] *School of Physics & Astronomy, Tel Aviv University, Ramat Aviv 69978, Israel*
[5] *Departments of Physics and Astronomy, University of California, Berkeley, CA 94720, USA*
[6] *Max-Planck-Institut für Astronomie, Königstuhl 17, 69117 Heidelberg, Germany*
[7] *Max-Planck-Institut für Astrophysik, Karl Schwarzschildstr. 1, D-85737 Garching, Germany*
[8] *Universitäts-Sternwarte, Ludwig-Maximilians-Universität München, Scheinerstr. 1, 81679 München, Germany*
[9] *Harvard-Smithsonian Center for Astrophysics, 60 Garden Street, Cambridge, MA 02138, USA*

Выборка модельных галактик

3.1 The TNG50 simulation

The TNG50 simulation (Nelson et al. 2019; Pillepich et al. 2019) is the highest-resolution volume of the IllustrisTNG project (Nelson et al. 2018; Naiman et al. 2018; Marinacci et al. 2018; Pillepich et al. 2018a; Springel et al. 2018), with a uniform periodic-boundary cube of 51.7 co-moving Mpc on a side, and 2×2160^3 initial resolution elements, half dark matter particles and half gas cells. The simulations are run with the unstructured moving-mesh code AREPO (Springel 2010) and incorporate dark matter, gas, stars, black holes, and magnetic fields. The dark matter and baryonic mass resolutions in TNG50 are $4.5 \times 10^5 M_\odot$ and $8.5 \times 10^4 M_\odot$, respectively, and the gravitational softening lengths at $z = 2$ are 192 pc for stars and dark matter, and adaptive for gas, with a typical size of $100 - 200$ pc for star-forming gas. The simulations account for star formation, stellar population evolution, chemical enrichment through supernovae type Ia and II and through AGB stars, gas radiative processes, the formation, coalescence, and growth of supermassive black holes, and feedback from supernovae and black holes (Weinberger et al. 2017; Pillepich et al. 2018b). TNG50 adopts a Planck Collaboration et al. (2016) cosmology with $h = 0.68$, $\Omega_b = 0.05$, $\Omega_m = 0.31$, $\Omega_\Lambda = 0.69$, and $\sigma_8 = 0.82$.

- Масса больше 40 млрд. масс Солнца
- Темпы звездообразования больше 50 масс Солнца в год; → 12 галактик из TNG50.
- Если выкинуть компактные и взаимодействующие, то 7 галактик

Вот они

Table 1. Physical properties of the TNG50 galaxies selected for kinematic analysis (top seven rows), and excluded (bottom 5 rows): stellar mass M_*, gas mass $M_{\rm gas}$, and instantaneous star formation rate SFR, all within a three-dimensional aperture with radius 20 kpc around the potential minimum, and the three-dimensional $K-$band half-light size $R_{1/2}$.

ID, subhalo (symbol)	M_* $[10^{11} M_\odot]$	$M_{\rm gas}$ $[10^{11} M_\odot]$	SFR $[M_\odot\ yr^{-1}]$	$R_{1/2}$ [kpc]
#1, 25822 (△)	1.0	0.6	71	2.0
#2, 39746 (⬠)	1.1	0.8	119	4.0
#3, 55107 (○)	1.5	1.0	113	3.7
#4, 60751 (▽)	0.5	0.5	48	6.2
#5, 79351 (◇)	1.2	0.6	92	3.2
#6, 92272 (◇)	0.5	0.3	70	2.1
#7, 99304 (□)	0.6	0.4	50	2.2
#8, 44316	0.9	0.7	309	0.7
#9, 50682	1.4	0.3	45	1.6
#10, 59076	0.9	0.3	66	1.5
#11, 74682	0.5	0.5	114	2.1
#12, 101499	0.9	0.2	65	0.5

Почти похожи на настоящие

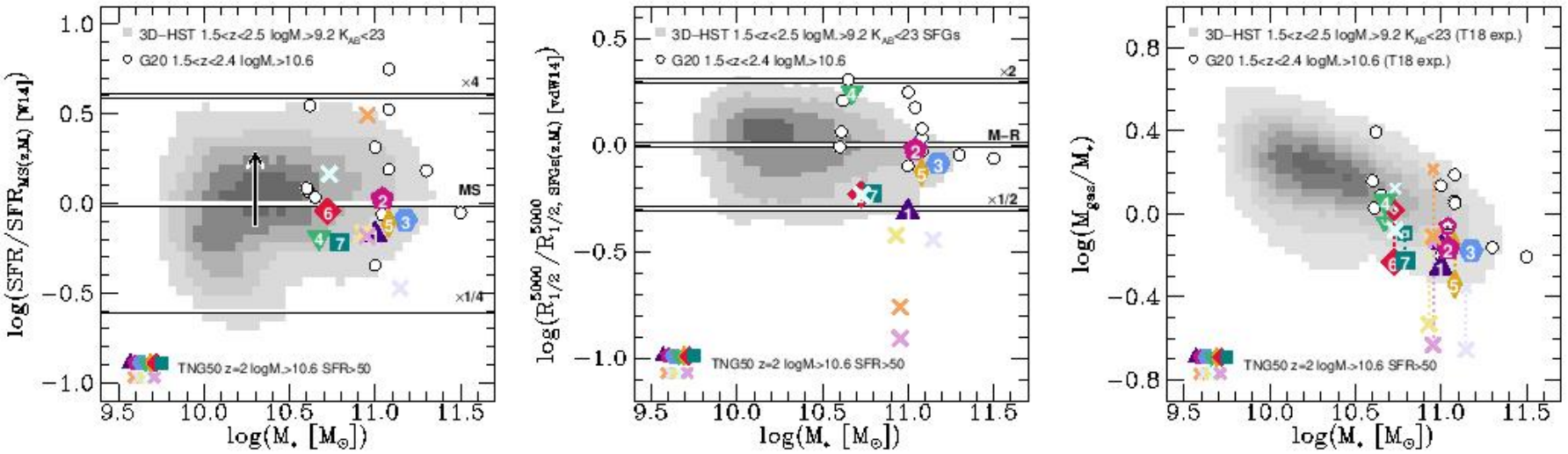

Figure 1. Intrinsic physical properties of TNG50 galaxies selected from the $z = 2$ snapshot with $M_* > 4{\times}10^{10} M_\odot$ and $\mathrm{SFR} > 50 M_\odot\ \mathrm{yr}^{-1}$ (colored symbols; cf. Table 1) in comparison to the observational reference sample by Genzel et al. (2020) (G20; white circles), and to the underlying observed galaxy population at $1.5 < z < 2.5$ based on the 3D-HST catalogue (grey scale; Brammer et al. 2012; Skelton et al. 2014; Momcheva et al. 2016). For the 3D-HST sample we apply the following cuts: $\log(M_*/M_\odot) > 9.2$, $K_{\mathrm{AB}} < 23$ mag, and for the middle panel also $\mathrm{SFR}/M_* > 0.7/t_{\mathrm{Hubble}}$. TNG50 galaxies that satisfy the stellar mass and SFR cuts but that are not included in the kinematic analysis (because undergoing a merger, disturbed or too compact, see main text) are shown as colored crosses. Masses and SFRs of the TNG50 galaxies are measured within a three-dimensional aperture with radius 20 kpc around the potential minimum. Offset from the main sequence (MS; left), offset from the mass–size relation ($M - R$; middle), and gas-to-stellar mass ratio (right) are shown as a function of stellar mass. In the left panel, the SFR is normalized to the MS as derived by Whitaker et al. (2014) at the redshift and stellar mass of each galaxy, using the redshift-interpolated parametrization by Wisnioski et al. (2015). The arrow indicates the difference between the Whitaker et al. (2014) main sequence normalization (applied for all data shown), and a normalization based on the TNG galaxies alone (Donnari et al. 2019a). In the middle panel, the half-light sizes are corrected to the rest-frame 5000 Å and normalized to the $M - R$ relation of SFGs as derived by van der Wel et al. (2014b) at the redshift and stellar mass of each galaxy. In the right panel, gas masses for the 3D-HST galaxies and the G20 sample are estimated from the scaling relations by Tacconi et al. (2018; T18). The smaller (open colored) symbols connected to the larger (filled colored) symbols indicate the values that would be expected for the TNG50 galaxies based on the T18 scaling relation.

Из них под 5 углами зрения сделали спектральные кубы, измерили кинематику газа и посчитали динамическую модель

To summarize, in our modeling setup we leave the following five parameters free, using flat or truncated Gaussian priors: the total baryonic mass $M_{\rm bar}$, the baryonic disc effective radius R_e, the baryonic bulge-to-total fraction B/T, the intrinsic velocity dispersion σ_0, and the total halo mass $M_{\rm halo}$. All other parameters are fixed, including the bulge effective radius, the bulge and disc Sérsic indices, inclination, and position angle. Also the dark matter halo profile shape is fixed, to either NFW, or to the individual, two-power density fits with free α and $\beta = 3$. For the observed galaxies, the best-fit parameters are as published by Genzel et al. (2020).

- Барионы: балдж плюс экспоненциальный диск
- Гало: Navarro-Frenk-White (NFW) или модифицированный NFW
- Изотропная, постоянная по радиусу дисперсия скоростей газа

«Внутренние» кривые вращения

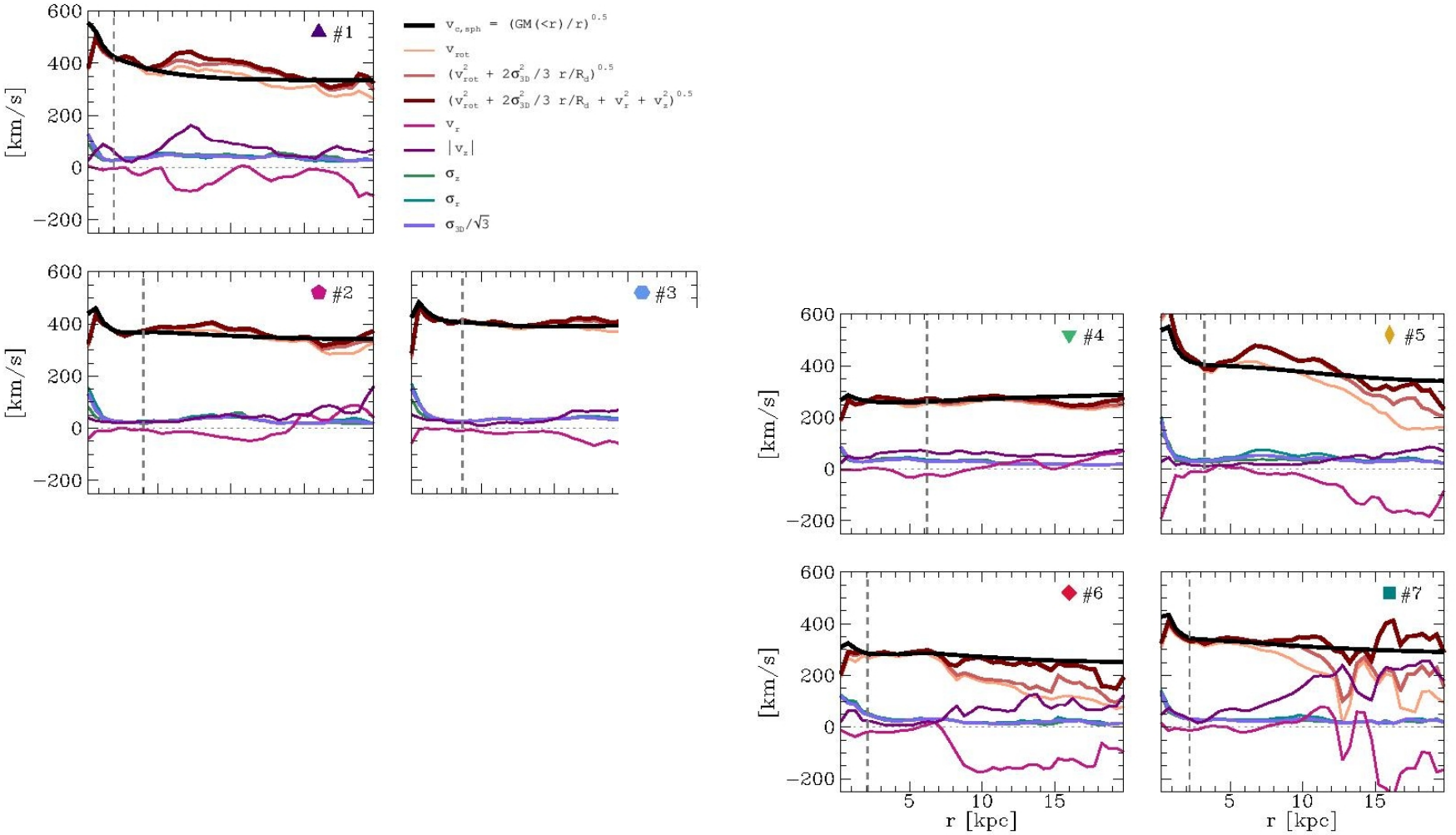

Figure 3. Different measures of the intrinsic velocity and velocity dispersion of a selection of TNG50 simulated galaxies, as indicated in the legend. The circular velocity $v_{c,sph}$ (black line) is calculated from the enclosed mass assuming spherical symmetry. The radial velocity dispersion σ_r (turquoise), vertical velocity dispersion σ_z (green), and three-dimensional velocity dispersion $\sigma_{3D}/\sqrt{3}$ (blue) are measured 'locally' in xy bins of 0.5 kpc length, and subsequently averaged, as is the vertical velocity component v_z (purple lines). All other properties are azimuthal averages. Light and dark brown lines show different corrections to the rotation velocity v_{rot} (salmon) from turbulent and other non-circular motions. Grey vertical dashed lines indicate the location of the stellar half-light radii (see Table 1).

А вот как эти кривые выглядят под 5ю углами зрения (i=60 deg)

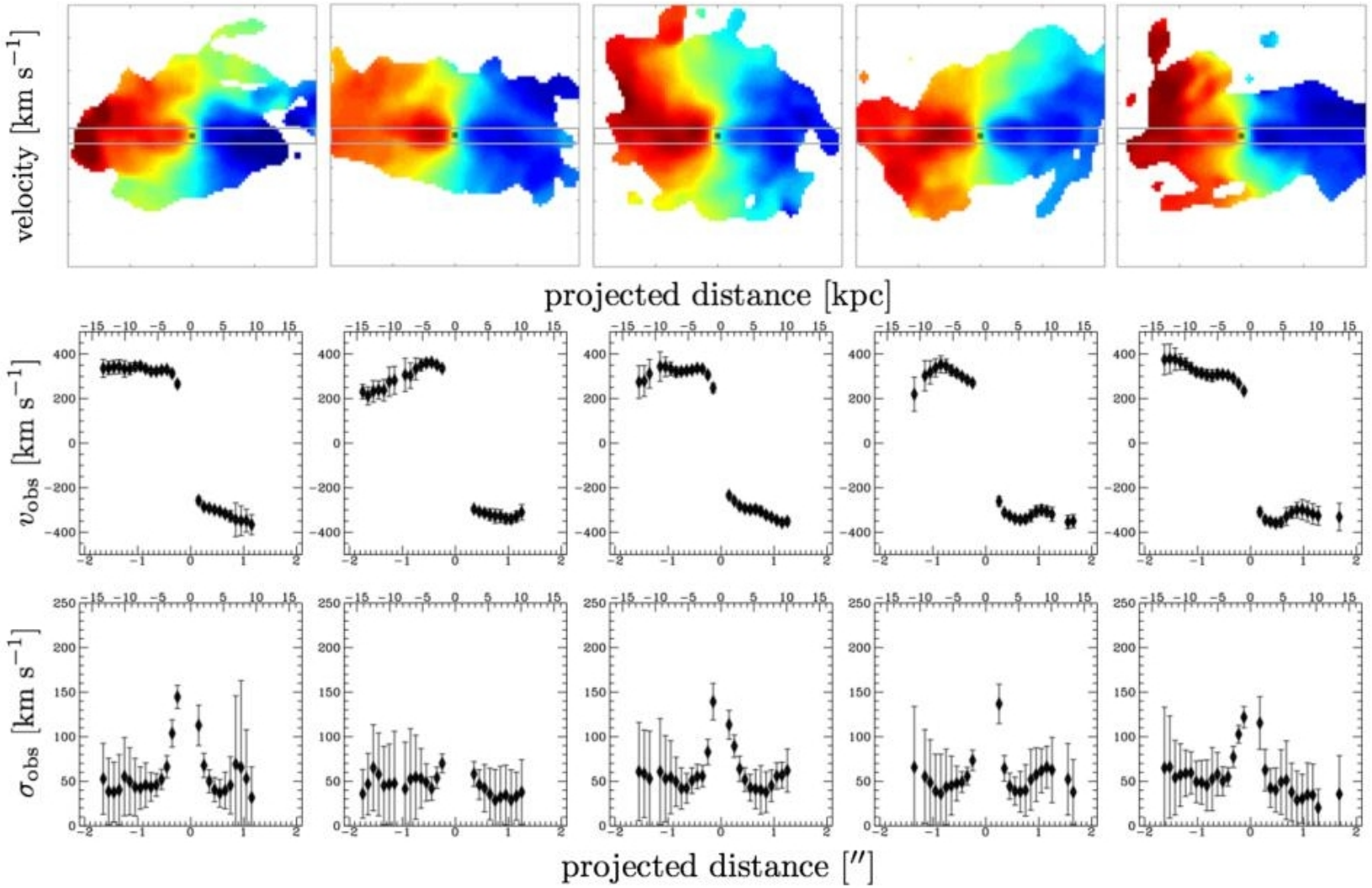

Сильная асимметрия! В отличие от реально наблюдаемых галактик

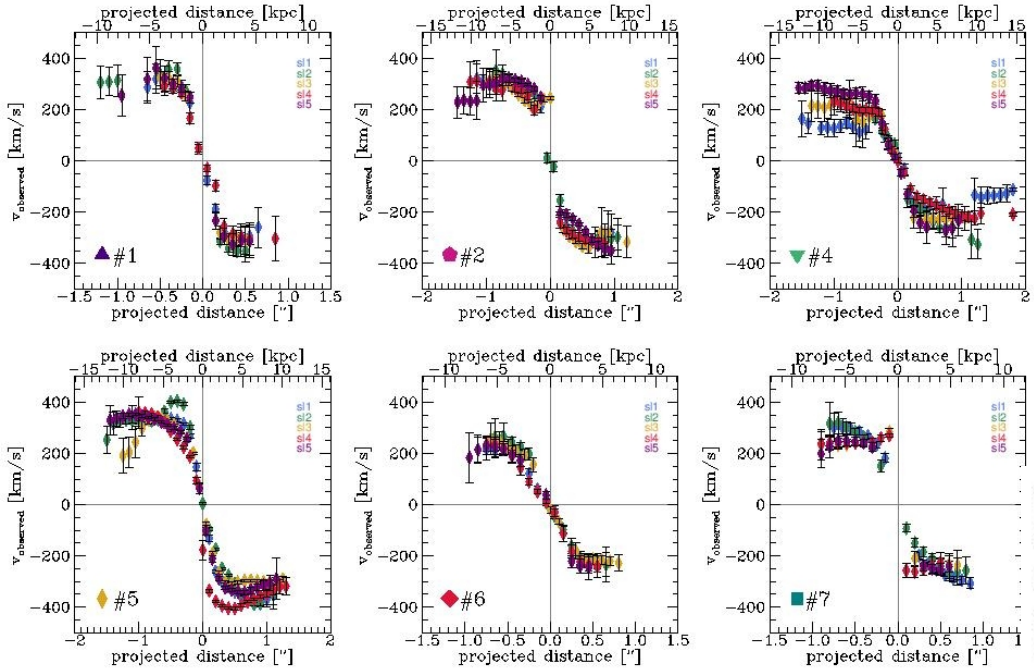

spond to both good fits and symmetric rotation curves. We find mean (median) $\Delta\chi^2_{\rm red} = 46.8$ (5.8) for the simulated galaxies, and mean (median) $\Delta\chi^2_{\rm red} = 2.1$ (1.6) for the G20 sample. Again, we repeat our calculations for fixed velocity uncertainties of $\delta v_{\rm rot} = \pm 10$ km s^{-1}. For the TNG50 galaxies, we find mean (median) $\Delta\chi^2_{\rm red} = 41.4$ (18.1), while for the G20 sample we find mean (median) $\Delta\chi^2_{\rm red} = 3.7$ (3.4). This test shows that the large $\Delta\chi^2_{\rm red}$ we find for the TNG50 galaxies is not due to S/N, but is because the rotation curves are less symmetric.

Both methods demonstrate that the simulated galaxies show large asymmetries in their rotation curves, and are less regular compared to the galaxies observed by Genzel et al. (2020).[7] For their full sample, Genzel et al. (2020) find that only 3/41 rotation curves show significant devia-

Доля темной материи – как восстановилась в модели

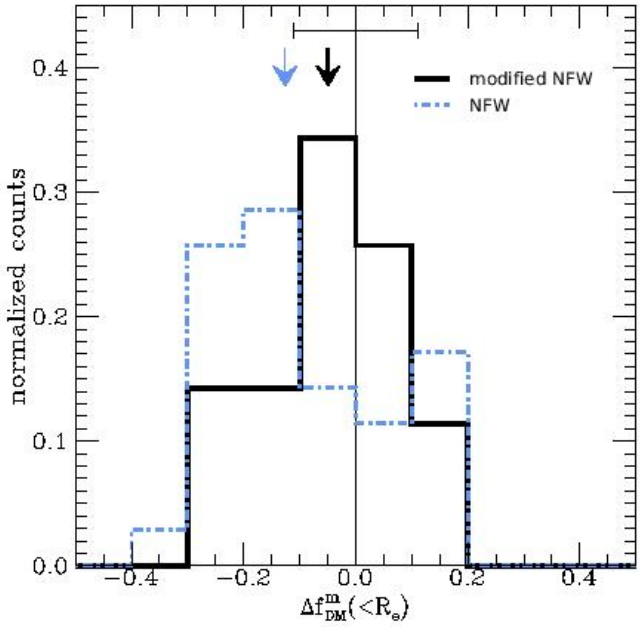

Figure 7. Difference in intrinsic *vs.* inferred central dark matter fractions $f^m_{\rm DM}(< R_e) = M_{\rm DM}(< R_e)/M_{\rm tot}(< R_e)$ based on the dynamical modeling of seven TNG50 simulated galaxies seen from five different projections each. The histograms show the distribution of $\Delta f^m_{\rm DM}(< R_e) = f^m_{\rm DM,fit}(< R_e) - f^m_{\rm DM,true}(< R_e)$ for fits with a modified NFW halo (black) and a pure NFW halo (blue dash-dotted), and the arrows indicate the median $\Delta f_{\rm DM}(< R_e)$. The error bar at the top gives the typical uncertainty on the central dark matter fraction for fits to observational data, $\delta f_{\rm DM}(< R_e) \approx \pm 0.11$. For our TNG50 galaxies, the model setup with a modified (i.e. contracted) NFW halo slightly underestimates the central dark matter fraction by 0.05 per cent on average, and the setup with an NFW halo by 0.13 per cent.

Начинаем сравнивать с наблюдениями: дисперсия скоростей

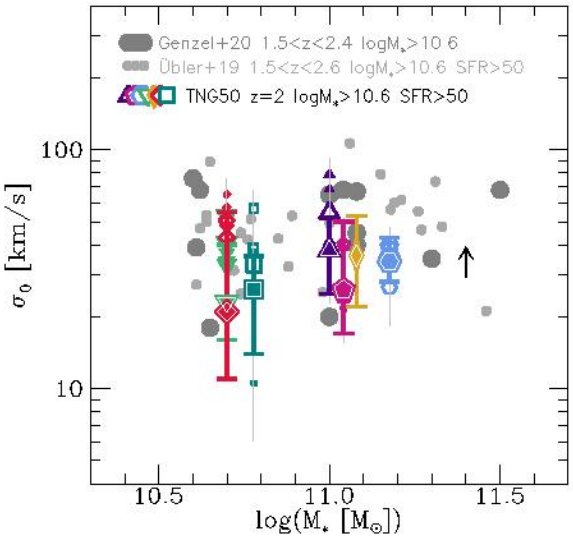

Figure 8. Gas velocity dispersion σ_0 as a function of intrinsic stellar mass M_* for the simulated galaxies selected from TNG50 at $z = 2$ (colored symbols), compared to the observational data by Genzel et al. (2020) (large grey circles) and Übler et al. (2019) (small light grey circles; see main text). Constraints from mock-observed and modelled galaxies are shown as open symbols, where larger sizes indicate higher goodness-of-fit. Filled symbols indicate the median of the intrinsic, azimuthally averaged 'local' velocity dispersion, and the corresponding error bar indicates the full range of values at distances $r = 1.5 - 20$ kpc. The black arrow approximately indicates (note the log scale) how far the intrinsic median values would increase if a 'thermal term' were included in the measurement of the velocity dispersion (see Pillepich et al.

Доля темной материи: все-таки в моделях выше. И радиус меньше!

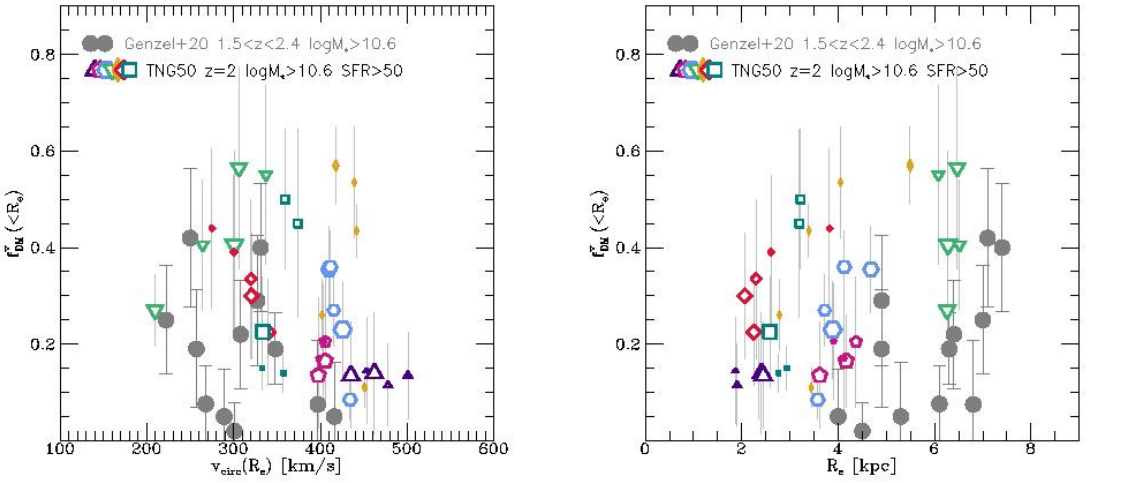

Figure 9. Left: Dark matter fraction within the baryonic disc effective radius $f^{v}_{\rm DM}(< R_e) = v^2_{\rm DM}(R_e)/v^2_{\rm circ}(R_e)$ as a function of circular velocity at the baryonic disc effective radius $v_{\rm circ}(R_e)$ for the selected simulated TNG50 galaxies at $z = 2$ with $M_* > 4 \times 10^{10} M_\odot$ and SFR $> 50 M_\odot$ yr^{-1} (colored symbols), in comparison to the selected observational data by Genzel et al. (2020) (grey circles). For the mock-observed and modelled TNG50 galaxies, larger sizes indicate higher goodness-of-fit (averaged over our setups with modified and unmodified NFW haloes). Within the modeling uncertainties, the simulated and observed populations largely overlap, but the simulated galaxies are offset towards higher velocities and dark matter fractions. Right: $f^{v}_{\rm DM}(< R_e)$ as a function of baryonic disc effective radius R_e, with symbols as in the left panel. Here we see a more distinct offset of the simulated and observed galaxies, where at fixed R_e the observed galaxies always have smaller dark matter fractions.

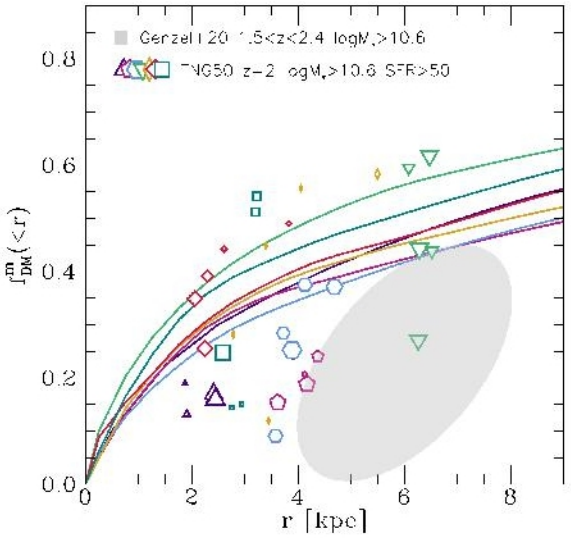

Figure 10. Enclosed dark matter fraction $f^{m}_{\rm DM}(< r) = M_{\rm DM}(< r)/M_{\rm tot}(< r)$ as a function of radius r. Colored lines show the intrinsic profiles of the seven TNG50 galaxies selected for this comparison at $z = 2$, and open colored symbols indicate the inferred $f^{m}_{\rm DM}(< R_e)$ from the modeled mock-observations. The grey shaded area indicates the approximate location of the selected observed galaxies by Genzel et al. (2020). All mock-observed and intrinsic low ($f^{m}_{\rm DM}(< R_e) < 0.2$) dark matter fractions are found for $R_e < 4.5$ kpc, in contrast to the observationally inferred values.

Чего уж мелочиться – вся выборка модельных галактик TNG50

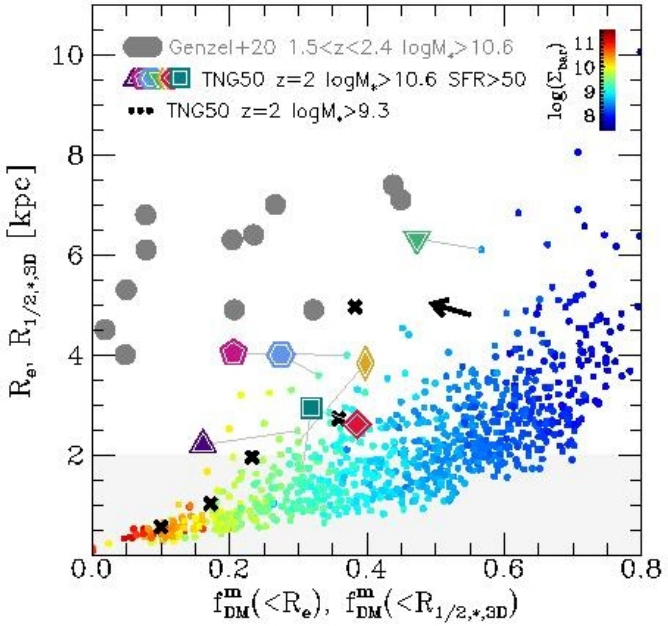

Figure 11. Baryonic disc effective radius R_e (three-dimensional stellar half-mass radius $R_{1/2,*,3D}$) as a function of enclosed dark matter mass fraction $f^m_{DM}(< r) = M_{DM}(< r)/M_{tot}(< r)$ at $r = R_e$ ($r = R_{1/2,*,3D}$). For the selected TNG50 galaxies we show model results averaged over five lines of sight and setups with/without a modified NFW halo (large colored symbols), with values based on R_e. Grey symbols show the massive, high$-z$ SFGs by Genzel et al. (2020), with values based on R_e. As small circles we show the full population of $M_* > 2 \times 10^9 M_\odot$ $z = 2$ galaxies in TNG50, color-coded by their baryonic surface density, with values based on $R_{1/2,*,3D}$. The black arrow indicates the average difference between values based on R_e (from our dynamical modeling) *vs.* $R_{1/2,*,3D}$ (intrinsic to the simulation) for the seven